ELSEVIER

Physics of the Earth and Planetary Interiors 88 (1995) 193–210

PHYSICS OF THE EARTH AND PLANETARY INTERIORS

# Absolute ionic diffusion in MgO—computer calculations via lattice dynamics

Lidunka Vočadlo [a,*], A. Wall [b], S.C. Parker [b], Geoffrey D. Price [a]

[a] *Research School of Geological and Geophysical Sciences, Birkbeck College and University College London, Gower Street, London WC1E 6BT, UK*

[b] *School of Chemistry, University of Bath, Claverton Down, Bath BA2 7AY, UK*

Received 15 April 1994; accepted 16 August 1994

**Abstract**

Computer calculations based upon lattice dynamics have enabled us to calculate self-diffusion coefficients ($D_{sd}$) in MgO, a significant component of the lower mantle. We have employed the supercell method to study the mechanisms governing the diffusion process thereby enabling us to calculate values for activation enthalpies and entropies for migration and formation. In the intrinsic regime we calculate

Magnesium: $D_{sd} = 2.20 \times 10^{-5} \exp\left(\frac{-5.70}{kT}\right)$

Oxygen: $D_{sd} = 1.24 \times 10^{-5} \exp\left(\frac{-5.72}{kT}\right)$

and in the extrinsic regime we calculate

Magnesium: $D_{sd} = N_V 2.84 \times 10^{-6} \exp\left(-\frac{1.985}{kT}\right)$

Oxygen: $D_{sd} = N_V 1.60 \times 10^{-6} \exp\left(-\frac{2.003}{kT}\right)$

where $N_V$ is the extrinsic defect concentration. We have also confirmed that for this system the diffusion path is not simple, but there is a predicted bifurcation of the saddle surface. Our results are comparable with previous embedded defect calculations, and suggest that current experimental data are unable to probe the intrinsic regime.

* Corresponding author.


*SSDI* 0031-9201(94)02987-3

## 1. Introduction

Magnesium oxide is the end member of the magnesiowüstite solid solution series ({Mg, Fe}O), a mineral prevalent in the Earth's deep interior. In order to gain some insight into the rheological properties of the lower mantle, an understanding of the mechanisms underlying solid-state transport in such mantle materials must be obtained. Therefore a study of the theoretical basis underlying the diffusion equation and its application to the relatively simple structure of MgO at conditions within the Earth's interior will further our knowledge of mass transport and energy flows in the mantle and thus will eventually provide us with further information concerning the dynamical properties of the Earth's deep interior.

Direct measurements of diffusion properties are extremely difficult to obtain, especially at the high temperatures and pressures required to simulate the Earth's interior. However, with reliable potential models and established methodology, computer modelling can enable us to perform calculations on almost any candidate mineral, to predict its bulk properties (free energy, heat capacity, incompressibility etc.), and can thereby lead to a more general picture of the dynamics, composition and evolution of the Earth's deep interior. In this paper we aim to establish the methodology needed to calculate ionic diffusion coefficients, and use Mg and O diffusion in MgO at ambient pressure as our exemplar.

At the macroscopic level diffusion is simply the flow of matter and energy; at the microscopic level, diffusion in a crystal lattice may be described by particle jumps over potential energy barriers within the minimum energy configuration of the lattice. In order to diffuse, an atom has to leave its position within the minimum energy configuration of the lattice, pass through a less stable higher energy position (not usually occupied by atoms) and then fall into a minimum energy position again either at another lattice site or between lattice sites. The probability of an atom overcoming such potential energy barriers is governed by statistical mechanics; as the atom vibrates about its equilibrium position, there is some probability that it will vibrate with a sufficiently large amplitude to jump out of its equilibrium position, after which it may either fall into a neighbouring vacant site or become trapped in a potential well between atoms at neighbouring sites. By simulating the motion of atoms in a crystal lattice and considering the pairwise forces between them, calculations may be performed in order to evaluate the free energy changes associated with such migrating ions.

In the following sections, we initially review the relevant diffusion equations, elucidating the quantities we wish to predict from our calculations. Following this, we present the background to the computer modelling of both perfect and defective systems, including a brief description of the techniques involved and the types of potentials used. We then apply Vineyard theory (Vineyard, 1957) and the potential model of Sangster and Stoneham (1981) to investigate ionic diffusion processes in MgO. We also investigate the effect on the energy surface resulting from the anharmonicity of the vibrational modes in the region of the saddle point. We show how this leads to bifurcation in the ⟨001⟩ direction, displacing the saddle point from its central position as the lowest energy diffusion route deviates from the most direct one. This effect becomes especially noticeable at high temperature, as the lattice expands. Therefore, we correct the Vineyard theory to accommodate this anharmonicity. Finally, we present results for Schottky defect and ion migration energies which enable us to calculate absolute ionic diffusion coefficients for both cation and anion diffusion in MgO.

## 2. The diffusion equations

For *face-centred* cubic crystals, such as MgO, the self-diffusion coefficient may be written

$$D_{sd} = D_V N_V \tag{1}$$

where $N_V$ is the atomic fraction of vacancies. $D_V$ is the coefficient for vacancy diffusion given by

$$D_V = \frac{Z}{6}\left(\frac{a}{\sqrt{2}}\right)^2 \upsilon \exp\left(\frac{\Delta S_m}{k}\right) \exp\left(-\frac{\Delta H_m}{kT}\right) \tag{2}$$

where $Z$ is the coordination environment of the diffusing species, $a$ is the cell parameter and $a/\sqrt{2}$ is the jump distance for MgO, $v$ is the attempt frequency, and $\Delta S_m$ and $\Delta H_m$ are the activation entropy and enthalpy of migration, respectively; $k$ is Boltzmann's constant and $T$ is the temperature in Kelvin (e.g. Poirier, 1985).

For lower temperature extrinsic diffusion, the atomic fraction of vacancies, $N_V$, is determined by trace element concentration (e.g. $3Mg^{2+} \leftrightharpoons 2Al^{3+} + \square$) or quenching effects; i.e. there are vacancies already present and the diffusion process involves only the migration of ions. For higher temperature intrinsic diffusion, defects are thermally generated. The equilibrium atomic fraction of intrinsically generated vacancies in a crystal structure, $N_V$, at a given temperature has an exponential dependence on the vacancy formation energy and is given by

$$N_V = \frac{n_V}{N} = \exp\left(\frac{\Delta S_f}{k}\right) \exp\left(-\frac{\Delta H_f}{kT}\right) \quad (3)$$

where $n_V$ is the number of vacant lattice sites, $N$ is the total number of lattice sites, $\Delta S_f$ is the formation entropy and $\Delta H_f$ is the formation enthalpy.

Therefore, substituting Eqs. (2) and (3) into Eq. (1) gives the intrinsic self-diffusion coefficient as

$$D_{sd} = \frac{Z}{6}\left(\frac{a}{\sqrt{2}}\right)^2 v \exp\left(\frac{\Delta S_f + \Delta S_m}{k}\right) \times \exp\left(\frac{-\Delta H_f - \Delta H_m}{kT}\right) \quad (4)$$

The problem we have therefore is to model these defect parameters and attempt frequencies. In both theory and experiment, the least well-constrained parameters in Eq. (4) are the entropy terms, $\Delta S_{sd} (= \Delta S_f + \Delta S_m)$, and the attempt frequency, $v$ (which is equivalent to the vibrational frequency of the migrating species along the migration path). In this paper, we use Vineyard theory which provides an alternative expression for $v \exp(\Delta S_m/k)$ in terms of the product of lattice vibrational frequencies, which we calculate for our interatomic potential model via quasi-harmonic lattice dynamical analysis, the basis of which is outlined below.

## 3. Computer simulation techniques

Computer modelling may be used to provide a microscopic understanding of the diffusion equation using lattice dynamical modelling. There are currently two approaches to simulating defects and diffusion in crystalline structures: the embedded defect method and the supercell method. Previous work on defect calculations (Sangster and Stoneham, 1984; Harding et al., 1987) employed the embedded defect method, in which a defect is modelled within a fixed volume as if it were in an infinitely extending lattice. In the supercell method employed in this paper, a single defect is introduced into a large unit cell with periodic boundary conditions such that the defect is repeated periodically. A constant pressure free energy minimisation calculation allows the structure to relax fully around the defect (Parker and Price, 1989); if the supercell is sufficiently large there will be little relaxation in the outer regions of the cell and defect–defect interaction will be minimised, thereby simulating an infinitely extending crystal lattice. In the limit, the results of the supercell method should be convergent with those obtained using the embedded defect approach once volume dilation has been taken into account.

### 3.1. The atomic model

The physical properties of a solid may be established by solving the Schrödinger equation explicitly, thereby obtaining precisely the energy surfaces associated with the interactions of electrons and nuclei within a given system. This ab initio approach is not universally practicable due to size and complexity of the required calculation. A simpler and more approximate treatment is provided through atomistic modelling which describes the interactions between atoms or ions within a crystal structure, as opposed to the finer details of each electronic interaction. Such an approximation is usually based upon the Born model of solids (Born and Huang, 1954) whereby only forces due to the electron clouds are included; the masses involved are too small for gravitational forces to be significant, and the level

of approximation excludes nuclear, strong and weak forces, but may be extended to include many-body effects.

In order to model such interatomic interactions, it is first necessary to understand the potential energy functions which describe them. This is achieved initially by considering a two-body system; many body systems are generally prohibitively complex, although simple three-body corrections may be included. When no net forces are acting on the constituent atoms, the sum of the attractive and repulsive potential energies between each pair of atoms in a crystalline solid at zero Kelvin is termed the static lattice energy:

$$U_L(r_{ij}) = \sum_{ij} \frac{q_i q_j}{r_{ij}} + \sum_{ij} \varphi_{ij} + \sum_{ijk} \theta_{ijk} \qquad (5)$$

The first term on the right-hand side is the contribution to the static lattice energy from the long-range Coulombic attraction for an infinite array of atoms. The second term accounts for the diffuse nature of the electron clouds surrounding the nucleus; it includes the short-range interactions associated with Pauli repulsion between neighbouring charge clouds, and the short- and long-range components of van der Waals attraction. The third term represents three-body interactions which, for severely ionic solids with dominant pairwise interactions, may be negligible.

In the rigid-ion model, the short-range interactions predominantly effect nearest neighbour ions. Short-range potential functions may be represented by pairwise potentials such as the Buckingham potential which takes the form

$$\varphi_{ij} = A_{ij} \exp\left(-\frac{r_{ij}}{B_{ij}}\right) - \frac{C_{ij}}{r_{ij}^6} \qquad (6)$$

where $A_{ij}$, $B_{ij}$ and $C_{ij}$ are constants and $r_{ij}$ is the interatomic separation. The first term in $\varphi_{ij}$ is that due to short-range repulsion, while the second is due to van der Waals induced dipole–dipole attraction.

In addition to the above, models may also include the shell description of ionic polarisability (Dick and Overhauser, 1958). In this, the ion (usually oxygen) is represented by a massless charged shell (representing the outer valence electron cloud) attached to a massive core by a harmonic spring, so that

$$U_s = \sum_i k_i^s r_i^2 \qquad (7)$$

where $k_i^s$ is the spring constant and $r_i$ is the core–shell separation. This gives a simple mechanical description of ionic polarisability, necessary for the calculation of defect energies and high frequency dielectric constants. The resulting free-ion polarisability is given by

$$\alpha_i = \sum_i \frac{(Y_i e)^2}{k_i^s} \qquad (8)$$

where $Y_i$ is the shell charge, and $e$ is the charge on the electron. The short-range potential parameters for the oxygen–oxygen and magnesium–oxygen interactions used in this study are given in Table 1 (Catlow et al., 1977).

Table 1
Parameters for the Buckingham short-range potential given by Eq. 6

| | $A$ (eV) | $B$(Å) | $C$(eVÅ$^6$) |
|---|---|---|---|
| $O^{2-}$–$O^{2-}$ | 22764.3 | 0.1490 | 20.37 |
| $Mg^{2+}$–$O^{2-}$ | 1275.2 | 0.3012 | - |

The oxygen ion shell model was used with a shell charge of $-2.82107$, a balancing core charge of $+0.82107$, and a spring constant of $k^s = 46.13$eV Å$^{-2}$; the magnesium ion polarisability was assumed to be negligible owing to its relatively small size.

The summation of the long-range Coulombic interactions in the potential energy function given by Eq. (5) is very slowly convergent, and therefore computationally time consuming and expensive. The PARAPOCS code used in this study (Parker and Price, 1989) employs the Ewald Method to calculate this Coulombic term (Ewald, 1921, 1937; Catlow and Norgett, 1978).

### 3.2. Perfect lattice simulations

Using interatomic potentials such as the ones described above, the code PARAPOCS (Parker and Price, 1989) enables the prediction of minimum energy structures at zero Kelvin. However,

above absolute zero atoms vibrate vigorously about their mean equilibrium lattice positions. This dynamic contribution to the energy of a crystal may be calculated in one of two ways: for medium- to high-temperature simulations, molecular dynamics is used (e.g. Dove, 1988) whilst for medium- to low-temperature simulations, lattice dynamics is more appropriate.

The lattice dynamics method is a semiclassical approach that uses the quasi-harmonic approximation to describe a cell in terms of independent quantised harmonic oscillators whose frequencies vary with cell volume, thus allowing for thermal expansion (e.g. Born and Huang, 1954). The motions of the individual particles are treated collectively as lattice vibrations or phonons. In PARAPOCS (see Parker and Price, 1989 for details), the phonon frequencies, $\omega(\boldsymbol{q})$, are obtained by solving

$$m\omega^2(\boldsymbol{q})e_i(\boldsymbol{q}) = \boldsymbol{D}(\boldsymbol{q})e_j(\boldsymbol{q}) \tag{9}$$

where the dynamical matrix, $\boldsymbol{D}(\boldsymbol{q})$, is defined by

$$\boldsymbol{D}(\boldsymbol{q}) = \sum_{ij}\left(\frac{\partial^2 U}{\partial \boldsymbol{u}_i \partial \boldsymbol{u}_j}\right)\exp(i\boldsymbol{q}\,\boldsymbol{R}_{ij}) \tag{10}$$

where $\boldsymbol{R}_{ij}$ is the interatomic separation and $\boldsymbol{u}_i$ and $\boldsymbol{u}_j$ are the atomic displacements from their equilibrium position. For a unit cell containing $N$ atoms, there are $3N$ eigenvalue solutions ($\omega^2(\boldsymbol{q})$) for a given wave vector $\boldsymbol{q}$. There are also $3N$ sets of eigenvectors ($e_x(\boldsymbol{q})$, $e_y(\boldsymbol{q})$, $e_z(\boldsymbol{q})$) which describe the pattern of atomic displacements for each normal mode. For ions interacting within the shell model, the cores and shells may be treated separately. Having calculated these predicted vibrational frequencies, a number of thermodynamic properties may be calculated, such as free energy and heat capacity, which are direct functions of these vibrational frequencies (e.g. Parker and Price, 1989).

### 3.3. The defective lattice

As mentioned above, modelling point defects in a crystal structure can be approached in one of two ways: a single defect, such as an ion vacancy, may be modelled in an infinitely extending lattice, or a defect may be modelled within an enlarged unit cell, a supercell, with repeating boundary conditions.

A defect embedded in an infinitely extending lattice structure can be described by the Mott-Littleton approach, which is the basis of codes such as CASCADE (Leslie, 1981). The lattice surrounding the defect is divided into two regions with a transition region between them. Region I is that in the immediate vicinity of the defect, containing maybe 100 ions, where the interaction energies are calculated explicitly for the relaxed, heavily distorted lattice; region II extends indefinitely away from region I and the energies associated with region II are calculated by more approximate continuum methods (Mott and Littleton, 1938).

In the supercell method, the defect is embedded within a 'grown' unit cell, containing several hundred ions, with periodic boundary conditions The energies are calculated via lattice dynamics, taking into account the defect–defect interactions between supercells. However, if the supercell is sufficiently large, there will be little distortion at the cell boundaries and the defect–defect interaction will be small enough so as to be negligible. The advantage this method has over the previous one is that the constant pressure, variable volume Gibbs free energy of the defective lattice may be calculated directly using the code PARAPOCS, permitting not only the calculation of defect enthalpies, but also the constant pressure entropic term. It is also possible to calculate the jump frequency of a particular defect.

### 3.4. Vineyard theory

There are several approaches to predicting the atomic jump frequencies of diffusing species. They can simply be estimated as being typical of lattice modes (i.e. $\sim 10^{13}$ s$^{-1}$) or they can be calculated from reaction rate theory, Green functions or dynamical theory (see, for example, Sangster and Stoneham, 1984). In this study we have chosen to use Vineyard theory, since it has proved successful in the past and is one of the more efficient methods for determining the pre-exponential factor in the diffusion equation.

Vineyard theory (Vineyard, 1957) is based upon absolute rate theory, and enables us to obtain an estimate for the attempt frequency, $v^*$, which is defined by

$$v^* = \frac{\prod_{j=1}^{N} \omega_j}{\prod_{j=1}^{N-1} \omega'_j} \tag{11}$$

where $\omega_j$ are the lattice frequencies with the defect in its stable state (i.e. one vacancy), and $\omega'_j$ are those of the defective lattice with the defect at the saddle point (i.e. two vacancies), thereby reducing the number of real (as opposed to imaginary) vibrational frequencies in the system to $N-1$; here $v^*$ is related to the attempt frequency, $v$, in the diffusion equation via

$$v^* = v \exp\left(\frac{\Delta S_m}{k}\right) \tag{12}$$

This relation is valid only within the harmonic approximation (Vineyard, 1957), since motions near the saddle point are treated by the theory of small oscillations, and therefore the anharmonicity that may arise at the saddle surface is not adequately treated and may require an anharmonic correction.

Thus for Mg or O diffusion in a phase such as MgO, diffusion is expected to be along the $\langle 110 \rangle$ direction, and the jump distance is therefore $a/\sqrt{2}$, where $a$ is the cubic cell parameter (see Fig. 1). The self-diffusion coefficient may be written, therefore, as

$$D_{sd} = \frac{Z}{6} N_V \left(\frac{a}{\sqrt{2}}\right)^2 v^* \exp\left(-\frac{\Delta H_m}{kT}\right) \tag{13}$$

where $N_V$ is the vacancy concentration. In order to calculate an absolute self-diffusion equation for $Mg^{2+}$ and $O^{2-}$ diffusion in MgO, we need to obtain appropriate values for $\Delta H_m$, $v^*$ and $N_V$.

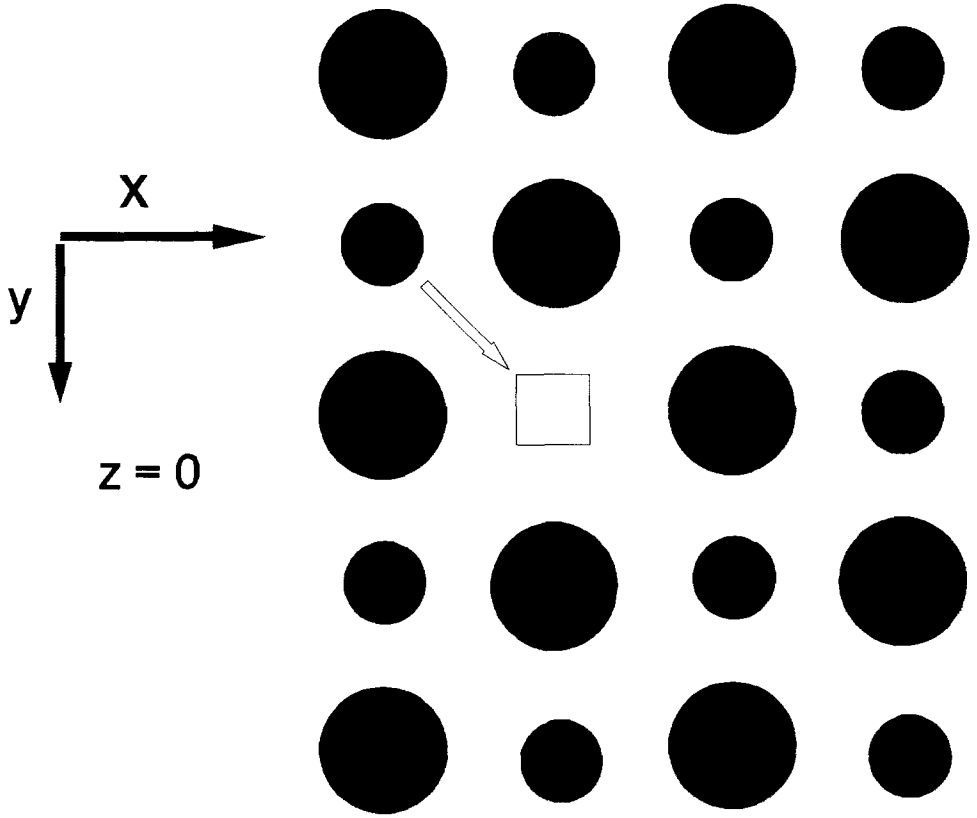


Fig. 1. Migration direction for ionic diffusion in MgO.

This we did for the interatomic potentials discussed above (Table 1), using the PARAPOCS code.

### 3.5. Sampling techniques

When performing a lattice dynamics calculation, ideally, one would like to sample all points within the first Brillouin zone of the crystal under investigation. However, such sampling is unfeasible since it would require infinite computer time and memory. The sampling points may be greatly reduced by symmetry but this still remains time consuming and expensive, so a number of averaging techniques have been developed (Baldereschi, 1973; Chadi and Cohen, 1973; Filippini et al., 1976). The degree of occupancy of phonon modes is highly temperature dependant. Above the Debye temperature, all modes are occupied and the sampling scheme is less important; however such high-temperature computer studies suffer because of the breakdown of the quasi-harmonic approximation as intrinsic anharmonicity becomes important. Below the Debye temperature, many more low-frequency modes are favoured and therefore the sampling technique employed becomes very relevant. The free energy of the crystal is a logarithmic function of phonon frequency and is therefore fairly robust to sampling; however the volume may well be affected. The Debye temperature for MgO is 942K and the calculations were performed well under this limit using one $q$-vector sampling at $q = \{1/4, 1/4, 1/4\}$, as recommended by Mills et al. (1991).

## 4. Results: calculation of $\Delta S_f$, $\Delta S_m$, $\Delta H_f$ and $\Delta H_m$

### 4.1. Supercell size

The choice of the size of the supercell was determined as a result of optimisation between modelling single defects in an infinitely extending perfect lattice (i.e. choosing an infinitely large supercell) and the problems involved with such large cells in terms of computer time. Table 2 shows how the enthalpy varies with cell size for both Schottky defect formation and cation migration, and the time involved for each calculation using the Convex Cluster at ULCC. For comparison, the embedded defect method using the computer code CASCADE gives a value of 7.5 eV for the Schottky formation energy (Mackrodt and Stewart, 1979), in very close agreement with the value obtained using our larger supercells. We chose to perform our simulations upon an MgO $3 \times 3 \times 3$ supercell containing 108 MgO units. This cell appears to give results which are convergent to within 0.1 eV of the embedded defect simulation, but which are not prohibitive in the amount of c.p.u. time required.

Table 2
The effect of supercell size on calculated defect energies

| Cell size (MgO units) | Schottky formation enthalpy (eV) | Cation migration enthalpy (eV) | C.p.u. time on convex (s) |
|---|---|---|---|
| 32 | 7.259 | 2.018 | 300 |
| 108 | 7.432 | 1.963 | 5000 |
| 125 | 7.509 | 1.956 | 7500 |
| 216 | 7.548 | 1.974 | 20000 |
| 256 | 7.531 | 1.979 | 30000 |

### 4.2. Schottky defect formation

The structure of MgO is one of dense ionic packing; because of this, Frenkel defects are energetically unfavourable, and so Schottky defects are the dominant source of intrinsic defects in MgO. The Gibbs free energy, volume and entropy of Schottky formation was calculated, using the $3 \times 3 \times 3$ MgO supercell containing 216 atoms, as a function of temperature; the results of our calculations over a simulated temperature range of 100–1000K are given in Table 3 and Fig. 2.

As mentioned above, we extrapolate a zero Kelvin formation enthalpy of 7.43 eV compared with the CASCADE value of 7.5 eV (Mackrodt and Stewart, 1979). This result does not seem to be strongly dependent upon the potential used, as Catlow et al. (1976), using a breathing shell model, obtained Schottky energies between 7.5 and 7.7 eV. We calculate a formation entropy

Table 3
Schottky formation parameters for MgO

| Temperature (K) | Formation energy (eV) | Formation volume ($cm^3\ mol^{-1}$) | Formation entropy (k) |
|---|---|---|---|
| 100 | 7.371 | 14.522 | 1.928 |
| 200 | 7.340 | 14.584 | 3.593 |
| 300 | 7.299 | 14.655 | 3.863 |
| 400 | 7.254 | 14.734 | 3.913 |
| 500 | 7.207 | 14.819 | 3.935 |
| 800 | 7.063 | 15.113 | 4.004 |
| 1000 | 6.963 | 15.349 | 4.084 |

which tends towards a high-temperature limit of approximately 4.1 k (Fig. 3).

Having calculated a formation enthalpy and entropy for Schottky defects in MgO, the next stage is to calculate an activation enthalpy and entropy for ionic migration to enable Eq. (13) to be evaluated.

### 4.3. Ion migration

The first requirement when trying to obtain ion migration energies is to establish where in the saddle energy surface the minimum energy configuration lies. With MgO this is not as simple as it may initially seem, for although MgO has a face-centred cubic crystal structure, the saddle point bifurcates as a function of cell volume, therefore making the problem much more complex. In PARAPOCS, the cell volume can be varied with temperature via the quasiharmonic approximation (Parker and Price, 1989). An ion may be fixed at an absolute position in space to

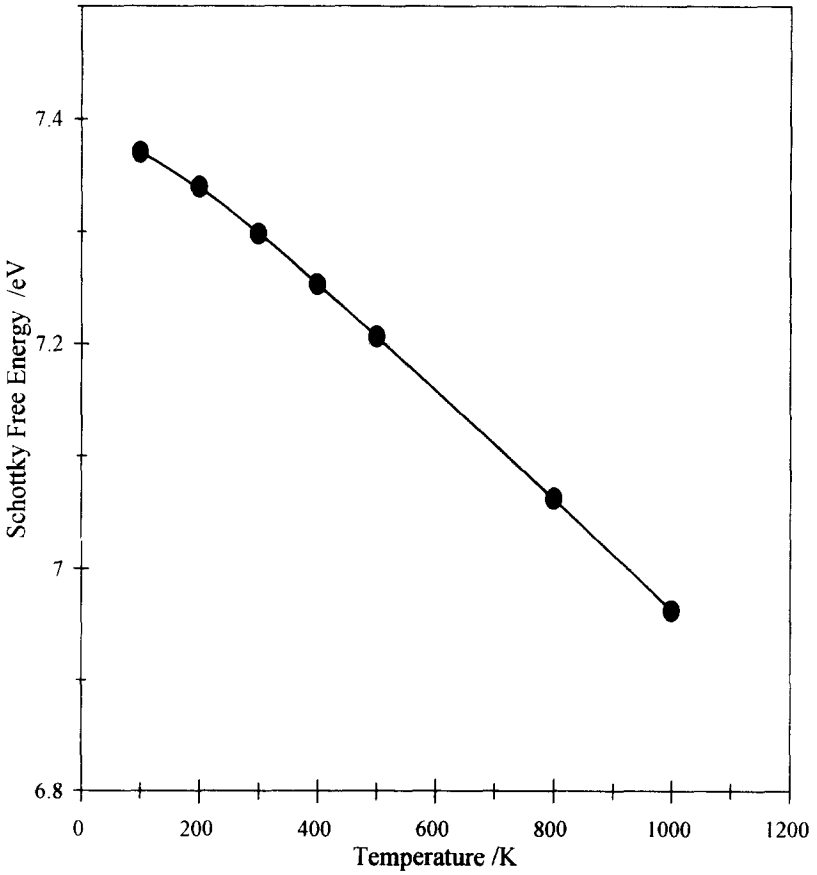


Fig. 2. Free energy vs. temperature for Schottky defect formation.

simulate the migration. At very low temperatures where the cell volume is at its smallest, the saddle surface is approximately harmonic in the ⟨001⟩ direction, but as the volume increases this energy surface bifurcates evolving into a double welled saddle surface with a maximum at its symmetric centre. In our calculations, placing an ion at this point would generate two imaginary frequencies: the first is expected, resulting from the energy maximum in the ⟨110⟩ direction—i.e. the jump direction; the second unstable vibrational mode results from the bifurcation with its principal motion being perpendicular to the jump path. The harmonic approximation fails at this point as an increasingly anharmonic, flattened saddle surface evolves with increasing volume.

The bifurcation described above is revealed by considering the potential well along the $z$ direction of the migrating ion (which is diffusing in the ⟨110⟩ direction) and performing a fixed volume calculation at increasing cell volumes (to simulate expansion with increasing temperature). The results of such calculations are shown in Figs. 4 and 5. These diagrams show how the potential energy well in the $z$ direction becomes increasingly unstable with increasing cell size and therefore temperature. It also shows that there is a local minimum at $z = 0$ for magnesium but a maximum at $z = 0$ for oxygen. In fact, as a consequence, the migrating oxygen defect would not minimise with this geometry. However, when placed at the local minimum (with the defect $z$-coordinate of 0.075

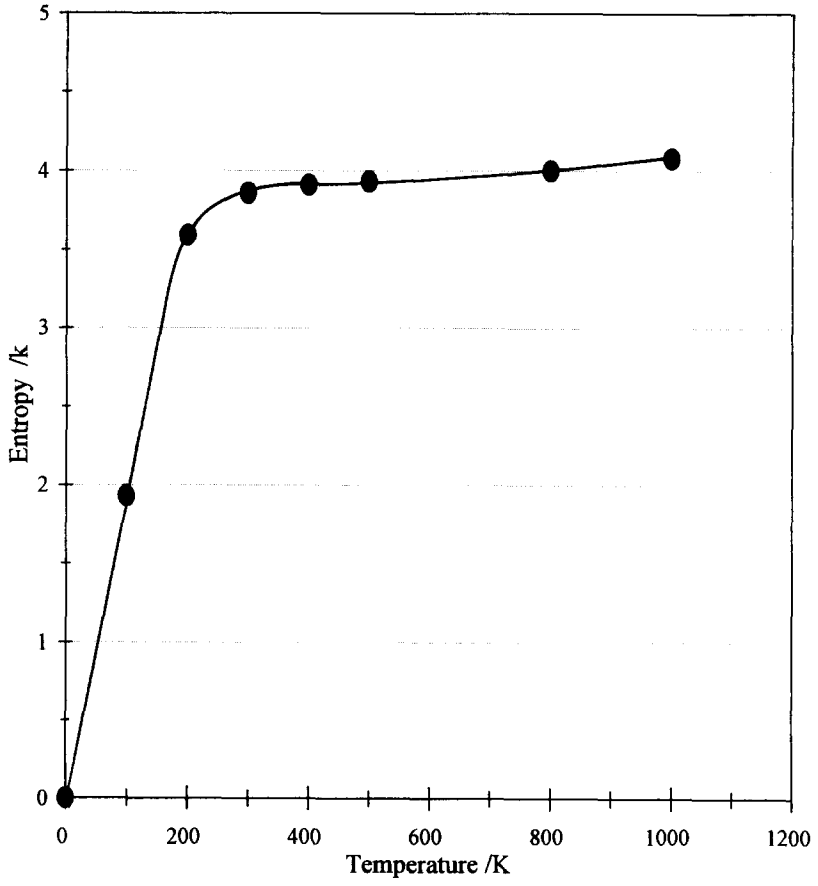


Fig. 3. Formation entropy vs. temperature for Schottky defect formation.

cell units), the lattice energy was successfully minimised and only the one desired imaginary frequency was predicted.

The migration free energy of $Mg^{2+}$ and $O^{2}$ in MgO was found as a function of temperature by fixing an ion midway between two vacant lattice sites in the $x = y$ direction (see Fig. 1) and, in the case of oxygen, off-centre in the $z$ direction. The free energy was calculated up to 400K for magnesium and 250K for oxygen after which the saddle surface bifurcates further and a secondary imaginary frequency appears. Results obtained from these simulations are shown in Tables 4 and 5, and Fig. 6.

Graphical extrapolation of the free energy (Fig. 6) to zero Kelvin yields an migration enthalpy of 1.985 eV for magnesium and 2.003 eV for oxygen. $\Delta S_m$ can be calculated from the slope of the free energy vs. temperature plot, and we calculate an migration entropy of 2.251 k for magnesium and 0.952 k for oxygen.

The quality of the predicted $\Delta H_m$ values can be gauged by comparing them with previous experimental or theoretical estimates of $\Delta H_m$, which include, for magnesium migration, 2.16 eV (Mackrodt and Stewart, 1979), 2.28 eV (Sempolinski and Kingery, 1980), 1.8–2.2 eV (Catlow and Norgett, 1976), 1.57–3.46 eV (Freer, 1980), and for oxygen diffusion, 2.38 eV (Mackrodt and Stewart, 1979), 1.3–2.1 eV (Catlow and Norgett, 1976).

The quality of our predicted $\Delta S_m$ values can only be gauged by comparing them with full diffusion coefficient data. In the following section, we

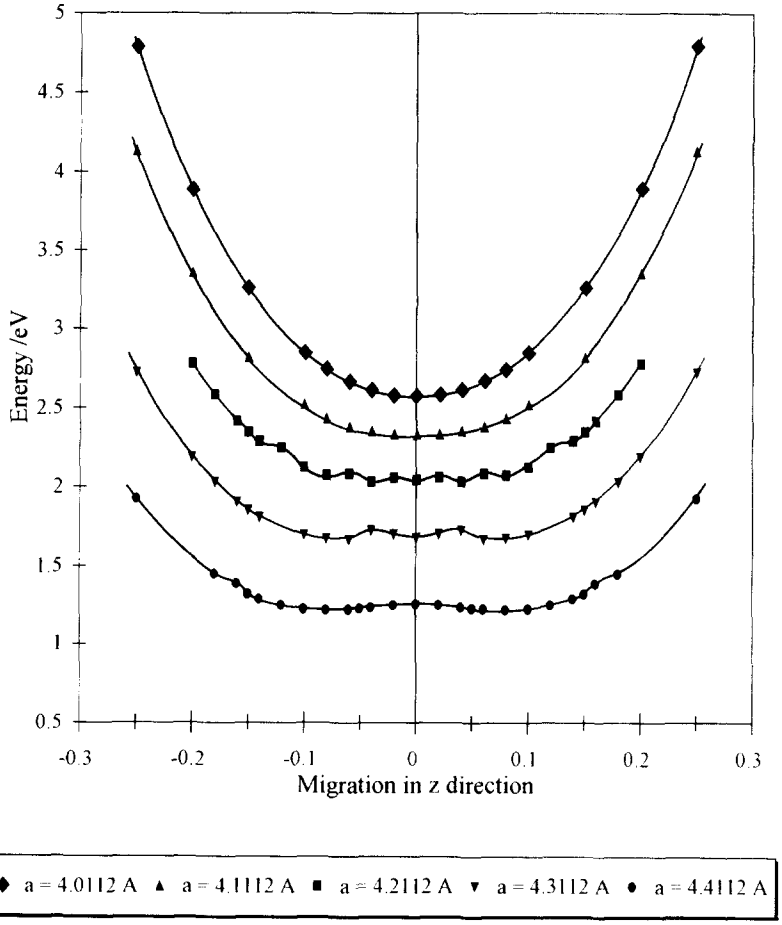


Fig. 4. Bifurcation of the magnesium saddle surface.

Table 4
Migration energy and migration volume for magnesium diffusion

| Temperature (K) | Migration energy (eV) | Migration volume ($cm^3\ mol^{-1}$) |
|---|---|---|
| 100 | 1.965 | 2.059 |
| 200 | 1.948 | 2.261 |
| 300 | 1.928 | 2.569 |
| 400 | 1.907 | 3.169 |

Table 5
Migration energy and migration volume for oxygen diffusion

| Temperature (K) | Migration energy (eV) | Migration volume ($cm^3\ mol^{-1}$) |
|---|---|---|
| 50 | 1.997 | 2.155 |
| 100 | 1.997 | 2.163 |
| 150 | 1.991 | 2.172 |
| 200 | 1.988 | 2.179 |
| 250 | 1.981 | 2.188 |

use Vineyard theory to calculate *absolute* diffusion coefficients which are then compared with experiment.

### 4.4. The attempt frequency via vineyard theory

The attempt frequency may be obtained using Vineyard theory (Eq. 11). Vineyard theory is a harmonic theory and therefore the eigenfrequencies of the 108 MgO unit supercell were calculated at 1 K in both the relaxed equilibrium and saddle point configurations of the defective lattice obtaining one imaginary frequency for the unstable migrating ion as required. This unstable mode, corresponding to the motion of the defect

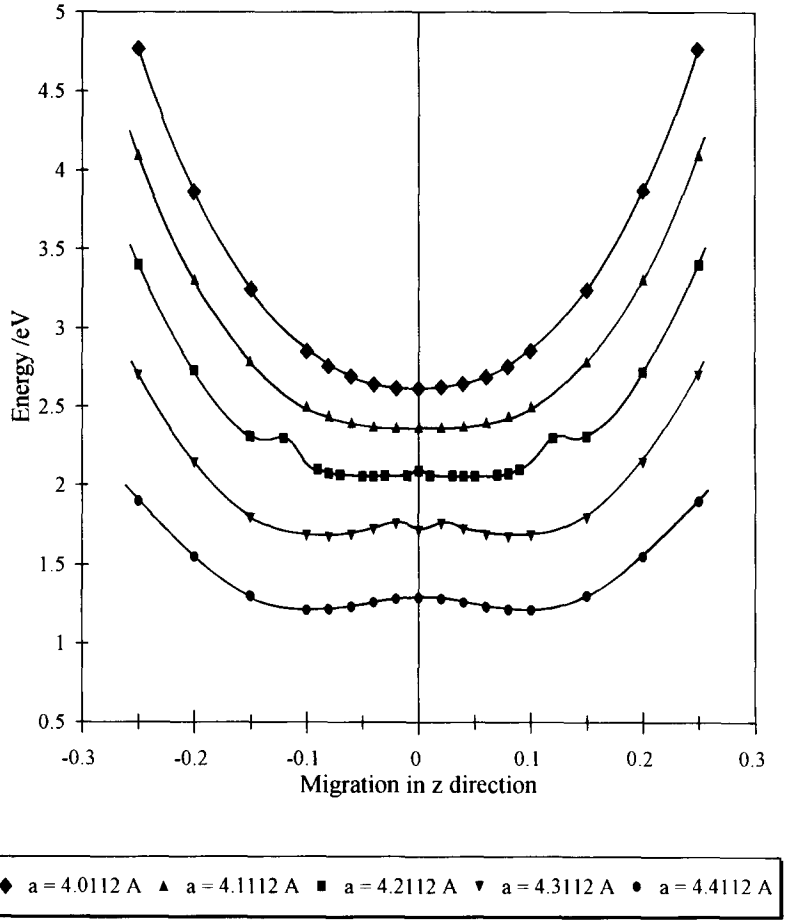


Fig. 5. Bifurcation of the oxygen saddle surface.

across the saddle plane, is excluded from the denominator in Eq. (11). From Vineyard theory we found that the harmonic attempt frequencies, $\upsilon^*$, for magnesium and oxygen diffusion were 18.99 THz and 9.83 THz, respectively. In fact, the attempt frequencies calculated from Vineyard theory are overestimated because of the low-frequency anharmonic mode at the saddle point associated with the displacement of the migrating ion in the ⟨001⟩ direction. Following Harding et al. (1987), this anharmonicity due to the incipient bifurcation needs to be corrected by applying a scaling factor to the results of the intrinsically harmonic Vineyard theory. The correction applied to the low frequency mode (see, for example, Sangster and Stoneham, 1984; Harding et al., 1987), reduces the calculated value of $\upsilon^*$. We have to find out how much the actual saddle surface in the $z$ direction differs from harmonic and apply numerical integration methods to determine the rescaling factor that needs to be incorporated in Vineyard theory.

Figs. 7 and 8 show the calculated migration energies at 1K for both the cation and anion fitted to a fourth-order polynomial compared to the harmonic equivalent. Following Harding et al.

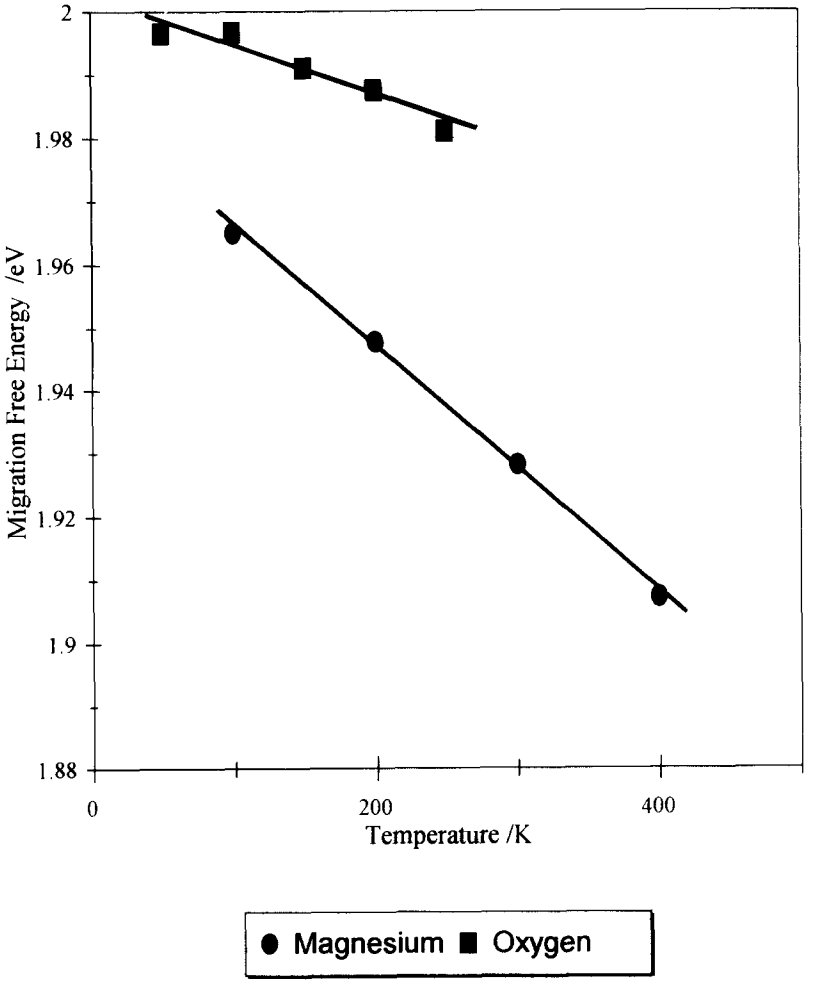


Fig. 6. Free energy vs. temperature for ionic migration.

(1987), the rescaling factor that needs to be applied to the values of $v^*$ predicted by Vineyard theory is given by

$$\frac{\int_0^{z_0} \exp\left(\frac{-E(z)}{kT}\right) dz}{\int_0^{\infty} \exp\left(\frac{-E'(z)}{kT}\right) dZ} \quad (14)$$

where $E(z)$ and $E'(z)$ are the calculated and harmonic energies respectively as a function of displacement $z$ away from the $\langle 110 \rangle$ direction to a maximum $z_0$, taken in this study to be when $z = 0.25$. This yields an estimate of the reduction factor which must be applied to Vineyard theory in the temperature range 100–2000 K of 0.99–0.84 for magnesium and 0.97–0.87 for oxygen (see Fig. 9). When accounting for this anharmonicity by applying the maximum correction, this reduces the attempt frequencies to 16 THz for the $Mg^{2+}$ ion and 9 THz for the $O^{2-}$ ion. Therefore, from Eq. (13) and taking $Z = 12$ for the diffusion of Mg and O in MgO, we obtain the following *extrinsic* self-diffusion coefficients

For Mg:

$$D_{sd} = \tfrac{12}{6} N_V 8.87 \times 10^{-20}\ 16 \times 10^{12} \exp\left(-\frac{1.985}{kT}\right) \quad (15)$$

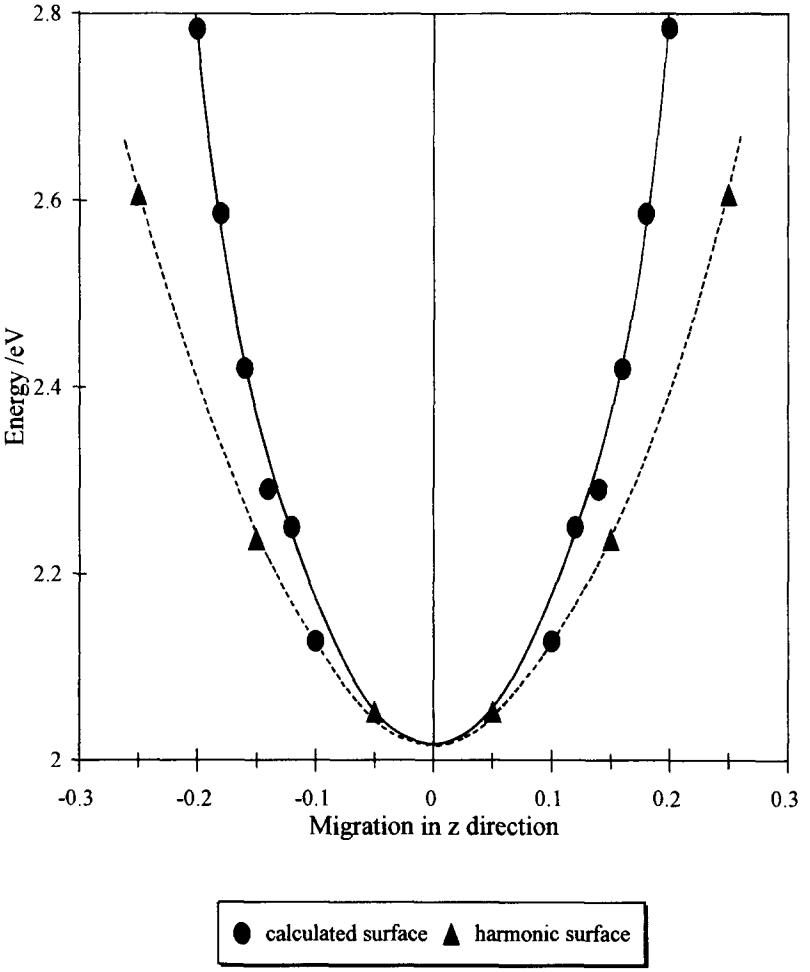


Fig. 7. Anharmonicity of saddle surface for magnesium.

$$= N_V 2.84 \times 10^{-6} \exp\left(-\frac{1.985}{kT}\right) \quad (16)$$

For O:

$$D_{sd} = \tfrac{12}{6} N_V 8.87 \times 10^{-20}\ 9 \times 10^{12} \exp\left(-\frac{2.003}{kT}\right) \quad (17)$$

$$= N_V 1.60 \times 10^{-6} \exp\left(-\frac{2.003}{kT}\right) \quad (18)$$

Table 6 summarises our results for the effective frequencies, the activation entropy and energy of migration, using the supercell method, compared to previous calculations using the same or similar potentials, but which used the embedded defect method. Sangster and Stoneham (1984) use Vineyard theory at constant volume to calculate the attempt frequencies; Harding et al. calculate $\upsilon^*$ from the activation entropy. It is not possible to compare our results directly with either of the two previous studies as Sangster and Stoneham (1984) use experimental data to infer $\Delta S_m$ (rather than the model predicted value used here), and Harding et al. (1987) use a different potential from the one used in our study. Nevertheless, the parameters for all pre-exponential terms in the table agree within one order of magnitude, which is probably as precise as one could hope for in any diffusion study. However,

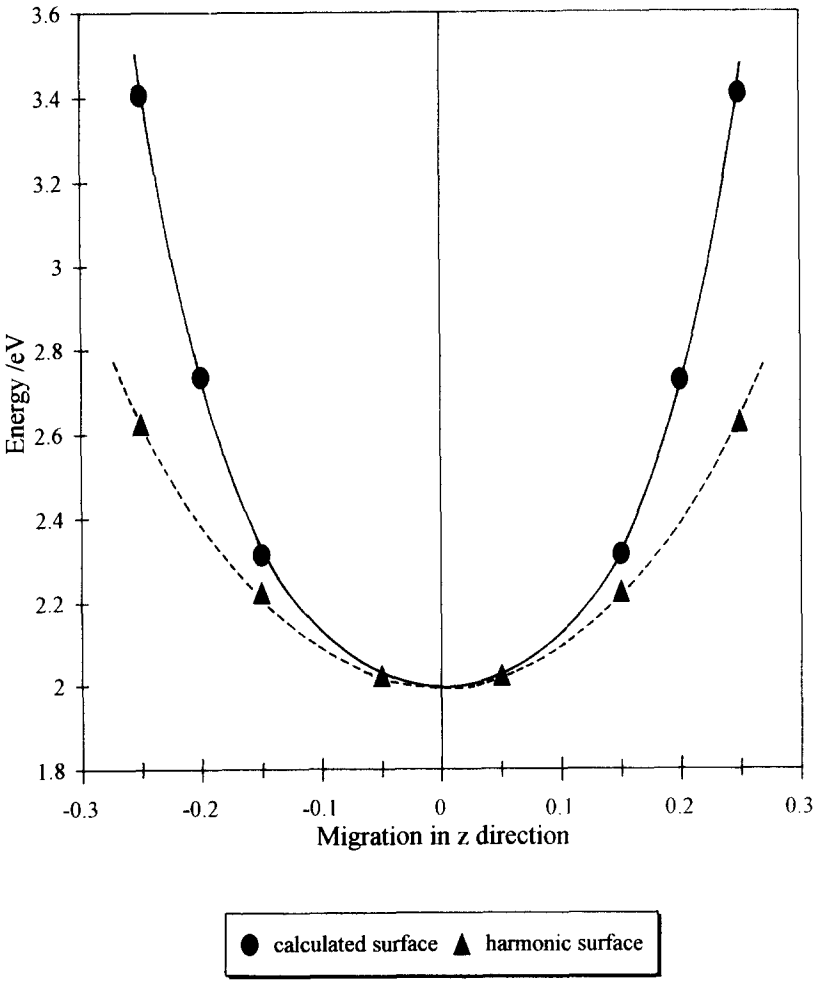


Fig. 8. Anharmonicity of saddle surface for oxygen.

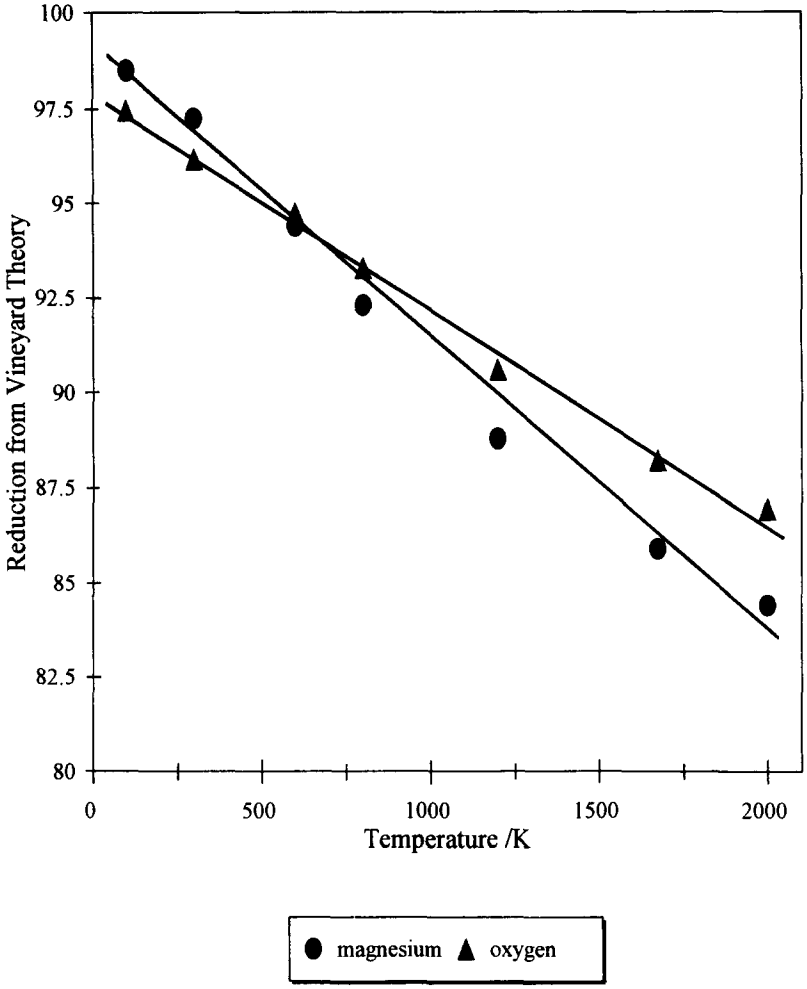


Fig. 9. Pre-exponential correction factors for magnesium and oxygen.

Table 6
Comparative diffusion parameters

| Source | | $\upsilon^*$ (THz) (from Vineyard theory) | Reduction factor | $\upsilon^*$ (THz) (with reduction factor) | $\Delta S_m/k_b$ (slope of free energy plot) | $\upsilon$ (THz) (from Eq. 12) | $\Delta H_m$ (eV) |
|---|---|---|---|---|---|---|---|
| Sangster and Stoneham (1984) (SS81 potential) Mg only | | 32.9 | 0.70 | 23.03 | 1.53 | 4.98 | 1.90 |
| Harding et al. (1987) (SS85 potential) Mg only | | 31.29 | 0.74 | 23.15 | 0.47 | 19.56 | 2.10 |
| This work | Magnesium | 18.99 | 0.84 | 15.95 | 2.25 | 1.69 | 1.98 |
| (SS81 potential) | Oxygen | 9.83 | 0.87 | 8.55 | 0.95 | 3.48 | 2.00 |

the activation enthalpies found in each case are in excellent agreement.

We can use the values of $\Delta H_f$ and $\Delta S_f$ to calculate the *intrinsic* diffusion coefficient, thus (remembering that the formation entropies and enthalpies take half the value of the Schottky defect formation energy)

For Mg:

$$D_{sd} = \tfrac{12}{6} \times 8.87 \times 10^{-20}\ 16 \times 10^{12} \times \exp\left(\frac{4.1}{2}\right) \exp\left(-\frac{\frac{7.43}{2} + 1.985}{kT}\right) \quad (19)$$

$$= 2.20 \times 10^{-5} \exp\left(\frac{-5.70}{kT}\right) \quad (20)$$

For O:

$$D_{sd} = \tfrac{12}{6} \times 8.87 \times 10^{-20}\ 9 \times 10^{12} \times \exp\left(\frac{4.1}{2}\right) \exp\left(-\frac{\frac{7.43}{2} + 2.003}{kT}\right) \quad (21)$$

$$= 1.24 \times 10^{-5} \exp\left(\frac{-5.72}{kT}\right) \quad (22)$$

Figs. 10 and 11 show how our calculated diffusion coefficients vary with temperature and how they compare with some experimental data (Freer, 1980). Our calculated extrinsic diffusion coefficient is plotted at different vacancy concentrations, $N_V = 1$, $10^{-2}$, $10^{-4}$, $10^{-6}$, and $10^{-8}$.

Our calculated results are in very close accord with experiment, and are compatible with materials having $N_V$ between about $10^{-3}$ and $10^{-7}$. Our results suggest that the intrinsic regime is only accessible at very high temperatures, implying that all experimental data currently available give quantitative values for extrinsic diffusion only. Our results indicate that it would be exceptionally difficult to generate defects intrinsically before melting ($T_m = 3120$K), since this would only be observed if $N_V < 10^{-6}$ and experiments were performed at more than 3000K. This conclusion has also been reached by Wuensch (1983) who considered diffusion in MgO in his extensive study of the results of experimental diffusion in close-packed oxides. From his research he found that both cation and anion diffusion in MgO was ill constrained with each experimental result plausible in its own right and dependent upon

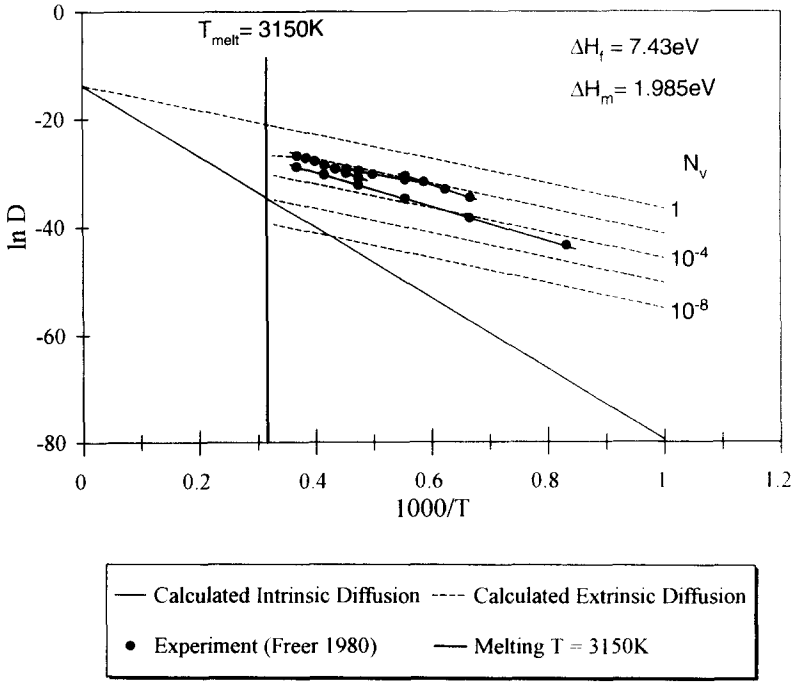


Fig. 10. Calculated absolute magnesium diffusion compared with experimental data.

experimental interpretation. He concluded that it was unlikely that any of the experiments he reviewed actually detected any intrinsic diffusion. It would seem apparent from this survey that computer calculations such as ours are necessary in order to provide a guide by which experimentalists may constrain their interpretations.

## 5. Conclusion

The supercell method for defect calculations used in the PARAPOCS computer code gives Schottky defect and ion migration energies which are comparable with those from the embedded defect code, CASCADE. When a reliable potential model is used, this gives quantitative agreement with experiment. The supercell method is preferable to the embedded defect method since the latter does not allow for dilation and this, therefore, requires various approximations to reduce the data to constant pressure conditions. The supercell method also allows for a migration route which deviates from the ⟨110⟩ direction as the saddle point shifts away from its central position. Applying an anharmonic correction to the predicted quasi-harmonic phonon frequencies allows us to calculate a viable attempt frequency using Vineyard theory which is comparable to that obtained from thermodynamical analysis of the free energy plots. The supercell method has enabled us to calculate both the extrinsic and intrinsic diffusion coefficient for ionic diffusion in MgO which may be used as a standard for evaluating defect concentrations experimentally. This paper supports the findings of Wuensch (1983) indicating that experimental techniques to date are only able to sample diffusion on MgO in the

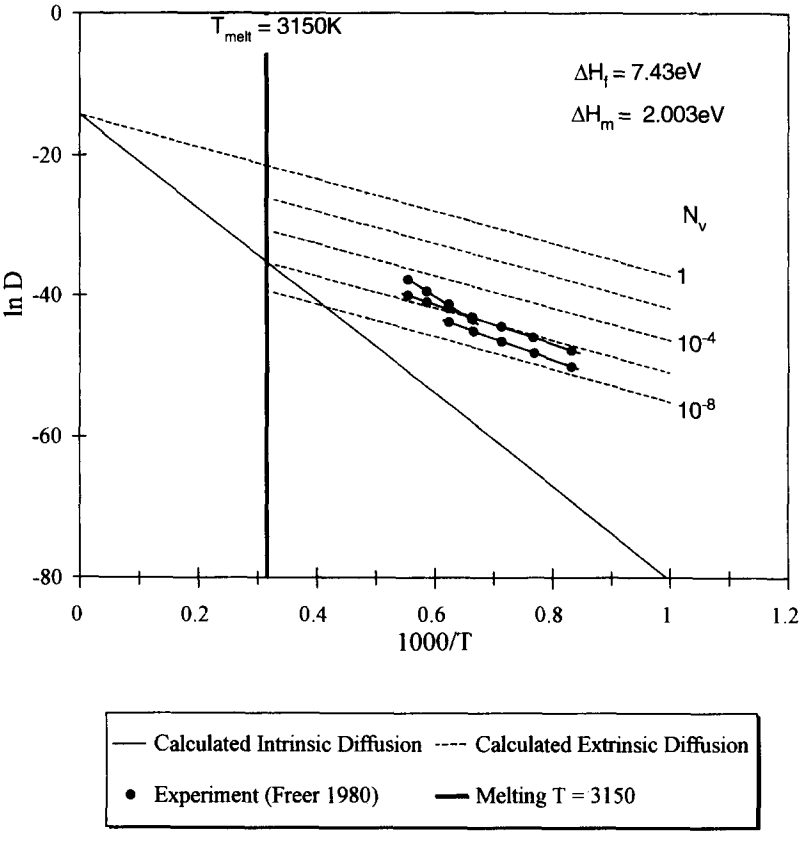


Fig. 11. Calculated absolute oxygen diffusion compared with experimental data.

extrinsic regime. Future research will focus upon simulating the effect of pressure on the free energy of defects and hence diffusion in mantle-forming phases.

## Acknowledgements

L.V. gratefully acknowledges the receipt of a NERC studentship, and G.D.P. thanks NERC for research grant GR3/6970. This is publication 48 of the UCL-Birkbeck Research School.

## References

Baldereschi, A., 1973. Mean value Point in the Brillouin Zone. Phys. Rev. B, 7: 5212–5215.

Born, M. and Huang, K., 1954. Dynamical Theory of Crystal Lattices. Oxford University Press, Oxford, UK.

Catlow, C.R.A. and Norgett, M.J., 1976. United Kingdom Atomic Energy Authority (UKAEA) Rep. AERE M2936. UKAEA, Harwell.

Catlow, C.R.A. and Norgett, M.J., 1978. United Kingdom Atomic Energy Authority (UKAEA) Rep. AERE M2763. UKAEA, Harwell.

Catlow, C.R.A., Faux, I.D. and Norgett, M.J., 1976. Shell and breathing model calculations for defect formation energies and volumes in magnesium oxide. J. Phys. C Solid St. Phys., 9: 419–429.

Catlow, C.R.A., Mackrodt, W.C., Norgett, M.J., and Stoneham, A.M., 1977. The basic atomic processes of corrosion. I: Electronic conduction in MnO, CaO and NO. Philos. Mag., 35: 177–187.

Chadi, D.J. and Cohen, M.L., 1973. Special points in the Brillouin Zone. Phys. Rev. B, 8: 5747–5753.

Dick, B.G. and Overhauser, A.W., 1958. Theory of the dielectric constants of Alkali halide crystals. Phys. Rev., 112: 90–103.

Dove, M., 1988. Molecular dynamics simulation in the solid state sciences. In: E.K.H. Salje (Editor). Physical Properties and Thermodynamic Behavior of Minerals. Reidel, Dordrecht, pp. 501–590.

Ewald, R.P. 1921. Die Berechnung Optischer, und Elektrostatischer Gitterpotentiale, Ann. Phys. 64: 253–287.

Ewald, R.P. 1937 Gottinger Nechr. Math-Phys. K1, 55.

Filippini, G., Gramaccioli, C.M., Simonetta, M. and Suffritti, G.B., 1976. Lattice dynamical applications to crystallographic problems: consideration of Brillouin Zone sampling. Acta Crystallogr., A32: 259–264.

Freer, R., 1980. Bibliography: self diffusion and impurity diffusion in oxides. J. Mater. Sci., 15: 803–824.

Harding, J.H., Sangster, M.J.L. and Stoneham, A.M., 1987. Cation diffusion in alkaline earth oxides. J. Phys. C: Solid State Phys., 20: 5281–5292.

Leslie, M., 1981. CCPS Report, SERC Daresbury Laboratory Rep. DL/SCI-TM31T.

Mackrodt, W.C. and Stewart, R.F., 1979. Defect properties of ionic solids: III. The calculation of the point defect structure of the alkaline earth oxies and CdO. J. Phys. C, 12: 5015–5036.

Mills, D.R., Parker, S.C. and Wall, A., 1991. The effect of pressure on Schottky pair formation in MgO: a lattice dynamical approach. Philos. Mag. A, 64: 1–12.

Mott, N.F. and Littleton, M.J., 1938. Conduction in polar crystals I. Electrolytic conduction in solid salts. Trans. Faraday Soc., 34: 485–499.

Parker, S.C. and Price, G.D., 1989. Computer modelling of phase transitions in Minerals. Adv. Solid State Chem., 1: 295–327.

Poirier, J.P., 1985. Creep of Crystals. Cambridge University Press, Cambridge, UK.

Sangster, M.J.L. and Stoneham, A.M., 1981. Calculations of off-centre displacements of divalent substitutional Ions in CaO, SrO and BaO from model potentials. Philos. Mag. B 43: 597–608.

Sangster, M.J.L. and Stoneham, A.M., 1984. Calculation of absolute diffusion rates in oxides. J. Phys. C: Solid State Phys., 17: 6093–6104.

Sempolinski, D.R. and Kingery, W.D., 1980. Ionic conductivity and magnesium vacancy mobility in magnesium oxide. J. Am. Ceram. Soc., 63: 664–672.

Vineyard, G.H., 1957. Frequency factors and isotope effects in solid state processes. J. Phys. Chem. Solids, 3: 121–127.

Wuensch, B.J., 1983. Diffusion in Stoichiometric Close-Packed Oxides. In: F. Bénière and C.R.A. Catlow (Editors), Mass Transport in Solids. NATO ASI Series, Plenum Press, New York, pp. 353–370.